

WILEY-VCH



European Chemical  
Societies Publishing

# Take Advantage and Publish Open Access



By publishing your paper open access, you'll be making it immediately freely available to anyone everywhere in the world.

That's maximum access and visibility worldwide with the same rigor of peer review you would expect from any high-quality journal.

**Submit your paper today.**



[www.chemistry-europe.org](http://www.chemistry-europe.org)



# Electronic Circular Dichroism Imaging (ECD<sub>i</sub>) Casts a New Light on the Origin of Solid-State Chiroptical Properties

Marcin Górecki,<sup>\*[a]</sup> Filippo Lipparini,<sup>[b]</sup> Gianluigi Albano,<sup>[b, d]</sup> Tamás Jávorfí,<sup>[c]</sup>  
Rohanah Hussain,<sup>[c]</sup> Giuliano Siligardi,<sup>[c]</sup> Gennaro Pescitelli,<sup>[b]</sup> and Lorenzo Di Bari<sup>\*[b]</sup>

*Dedicated to Professor Hans-Georg Kuball on the occasion of his 90th birthday.*

**Abstract:** Solid-state ECD (ss-ECD) spectra of a model microcrystalline solid, finasteride, dispersed into a KCl pellet were recorded by using the synchrotron radiation source at the Diamond B23 beamline. Scanning a surface of 36 mm<sup>2</sup> with a step of 0.5 mm, we measured a set of ECD imaging (ECD<sub>i</sub>) spectra very different from each other and from the ss-ECD recorded with a bench-top instrument (1 cm<sup>2</sup> area). This is due to the anisotropic part of the ECD (ACD), which averages to zero in solution or on a large number of randomly oriented crystallites, but can otherwise be extremely large. Two-way

singular value decomposition (SVD) analysis, through experimental and simulated TDDFT spectra, disclosed that the measured and theoretical principal components are in line with each other. This finding demonstrates that the observed isotropic ss-ECD spectrum is governed by the anisotropy of locally oriented crystals. It also introduces a new quality for ss-ECD measurements and opens a new future for probing and mapping chiral materials in the solid state such as active pharmaceutical ingredients (APIs).

## Introduction

Electronic circular dichroism (ECD) is one of the main tools for the determination of the absolute configuration of small molecules,<sup>[1]</sup> notably chiral active pharmaceutical ingredients (APIs)<sup>[2]</sup> and natural products.<sup>[1,3]</sup> Depending on the molecular structure, it can have high sensitivity to monitor and characterize even the smallest molecular stereochemical details both in solution and in the solid state. This is the reason why ECD is also largely applied to biophysical studies.<sup>[4]</sup> It also provides unique information on the supramolecular chirality,<sup>[5]</sup> that has great importance in chemistry, physics and materials science. The development of sophisticated theoretical computational models coupled with an increased power of computing

hardware has made the ECD approach even more relevant.<sup>[6]</sup> Not surprisingly, ECD, in comparison to other manifestations of natural optical activity, is nowadays the most deeply explored spectroscopy within the realm of chiroptical methods, both from the theoretical and the experimental points of view.<sup>[3b]</sup>

Using bench-top ECD instruments, a divergent incident light beam usually irradiates a large area of the sample of about 1 cm<sup>2</sup>. For this reason, any spectrum recorded by using a bench-top ECD spectropolarimeter represents an average of the chiroptical properties of a huge ensemble of investigated molecules. This has no consequence for isotropic liquid solutions that constitute the majority of measurements. However, this is not the case for inherently non-homogeneous samples in the solid phase as thin films or pellets.<sup>[7]</sup> Measuring the ECD in the solid state of a large area has two consequences: first, the structural information related to small domains (size of ~100 μm and below) is entirely lost; second, spectral artifacts due to local anisotropies, in particular linear dichroism (LD), and linear birefringence (LB) can be present and cannot be discriminated. The recent development of ECD imaging (ECD<sub>i</sub>) pioneered at the Diamond B23 beamline<sup>[8]</sup> has enabled the mapping of large sample surfaces at various spectral resolutions down to 0.01 mm<sup>2</sup> because of the highly collimated micro light beam of B23 beamline. Applications of ECD<sub>i</sub> have revealed the polymorphism of thin films of organic semiconductors and optoelectronic materials enabling the discrimination of different supramolecular architectures, possibly related to multiple aggregation pathways, within the areas investigated.<sup>[7]</sup>


To our knowledge, the ECD<sub>i</sub> method has not been applied yet to characterize the chiroptical properties of pellets made of finely grounded crystalline molecules, in this case an active pharmaceutical ingredient (API) mixed with an inert salt such as

[a] Dr. M. Górecki  
Institute of Organic Chemistry  
Polish Academy of Sciences  
ul. Kasprzaka 44/52, 01-224 Warsaw (Poland)  
E-mail: marcin.gorecki@icho.edu.pl

[b] Dr. F. Lipparini, Dr. G. Albano, Prof. G. Pescitelli, Prof. L. Di Bari  
Dipartimento di Chimica e Chimica Industriale  
Università di Pisa  
via Moruzzi 13, 56124 Pisa (Italy)  
E-mail: lorenzo.dibari@unipi.it

[c] Dr. T. Jávorfí, Dr. R. Hussain, Dr. G. Siligardi  
Diamond Light Source, Ltd.  
Chilton, Didcot, Oxfordshire OX11 0DE (UK)

[d] Dr. G. Albano  
Present address: Dipartimento di Chimica  
Università degli Studi di Bari "Aldo Moro"  
via Edoardo Orabona 4, 70126 Bari (Italy)

 Supporting information for this article is available on the WWW under <https://doi.org/10.1002/chem.202103632>

KCl.<sup>[3a,9]</sup> These specimens were composed of microcrystallites of various sizes and orientations isotropically distributed in the pellet (Figure 1).

In general, light passing through a region of the pellet devoid of any microcrystallite will show no ECD. It is important to note that the signal intensity and sign of the ECD of each microcrystallite will depend on its orientation relative to that of the propagation of incident light. The interaction of circularly polarized light (CPL) with chiral samples in isotropic media produces isotropic CD reported as a pseudoscalar quantity  $\Delta\varepsilon$ . The interaction of CPL with oriented samples produces instead anisotropic CD (ACD) which is described by a second-rank pseudotensor with elements  $\Delta\varepsilon_{\alpha\beta}$  ( $\alpha, \beta = 1, 2, 3$ ).<sup>[10]</sup> The isotropic CD is determined as follows:

$$\Delta\varepsilon = \varepsilon_L - \varepsilon_R = \frac{1}{3}(\Delta\varepsilon_{11} + \Delta\varepsilon_{22} + \Delta\varepsilon_{33}) \quad (1)$$

where  $\varepsilon_L$  and  $\varepsilon_R$  are the molar extinction coefficients for left- and right-CPL, and the three  $\Delta\varepsilon_{\alpha\alpha}$  are the diagonal elements of the ECD tensor. Upon randomized orientation, such as in solution, the measured CD amounts to the trace of the tensor expressed in Equation (1). The same should in principle hold for measurements of pellets, where all possible molecular orientations are averaged when the whole area is irradiated by the large cross section of the incident light of bench-top CD instruments. For that reason, one would expect ECD spectra measured in solution and in the solid-state of relatively rigid organic molecules to be qualitatively similar. There are, however, at least three reasons why this might not be the case: i) the existence of intermolecular interactions generating exciton couplings between closely packed chromophores of the molecules in the crystals;<sup>[11]</sup> ii) the impact of artifacts due to LD and LB contributions that might couple with instrumental defects;<sup>[12]</sup> and iii) the role of the electric dipole-electric quadrupole contribution ( $\mu Q$ ) to the rotational strength.<sup>[13]</sup> For isotropic samples, the latter term vanishes, and the rotational strength is

only determined by the electric dipole-magnetic dipole ( $\mu M$ ) contribution. For oriented samples in the solid state the  $\mu Q$  contribution survives, and each tensor element may be partitioned into two components:

$$\Delta\varepsilon_{\alpha\beta} = \Delta\varepsilon_{\alpha\beta}^{\mu M} + \Delta\varepsilon_{\alpha\beta}^{\mu Q} \quad (2)$$

It must be stressed at this point that not only  $\Delta\varepsilon$  but each term  $\Delta\varepsilon_{\alpha\beta}$  in Equation (1), and possibly its components, the electric dipole-magnetic dipole ( $\mu M$ ) and  $\mu Q$  of Equation (2), are conceivably sources of structural information, both qualitatively for stereochemical fingerprint and quantitatively for theoretical calculations/simulations. Each term will have its own sign and intensity for each electronic transition for a given enantiomer. This information, obviously lost for molecules in solution or in isotropic solid-state pellet, can be recovered using oriented samples. This method has been pioneered by Kuball, who investigated a vast number of organic compounds embedded in cholesteric phases,<sup>[14]</sup> and further developed by Watarai for a thin film of chiral DNA samples on glass and kidney bean leaf.<sup>[15]</sup> Unfortunately, it has many disadvantages including the use of specialized equipment capable of measuring the precise sample orientation, the necessity of recording spectra for several distinct orientations, the need for obtaining order parameters from independent methods such as NMR, and the fact that the decomposition into  $\mu M$  and  $\mu Q$  components cannot be achieved experimentally. More recently, ACD spectra have been measured and theoretically reproduced for oriented protein-pigment complexes, providing much richer structural information than the isotropic CD spectra.<sup>[16]</sup>

As a model compound, we have studied pellets prepared from fine ground crystals of form I of finasteride (Figure 1), a drug used for the treatment of male pattern hair loss and benign prostatic hypertrophy,<sup>[17]</sup> mixed with KCl, using a bench-top CD instrument and the highly collimated microbeam of B23 beamline of the Diamond Light Source synchrotron for CD imaging.<sup>[7a,8]</sup> The aims of this ECD imaging study were the following: 1) to ascertain the role and possible impact of local anisotropies in the solid state by imaging the grid area of the pellet at high spatial resolution of about 100  $\mu m$ ; 2) to verify that the average over an ensemble representing all possible crystal orientations coincides with the conventional solid-state ECD spectrum and is therefore a true chirality measurement,<sup>[10,14b]</sup> which can be used to assign the absolute configuration; and 3) to develop a new methodology to extract additional information from microcrystalline samples, without the need of orienting the sample specimens and of single large crystals (side  $\geq 2$  mm). Our findings obtained from a synergy between experimental ECDi data obtained using the highly collimated microbeam of B23 beamline<sup>[7a]</sup> and a theoretical approach for calculating isotropic CD and ACD spectral components paved the way for the characterization of the chiroptical properties of chiral molecules in the crystal form.

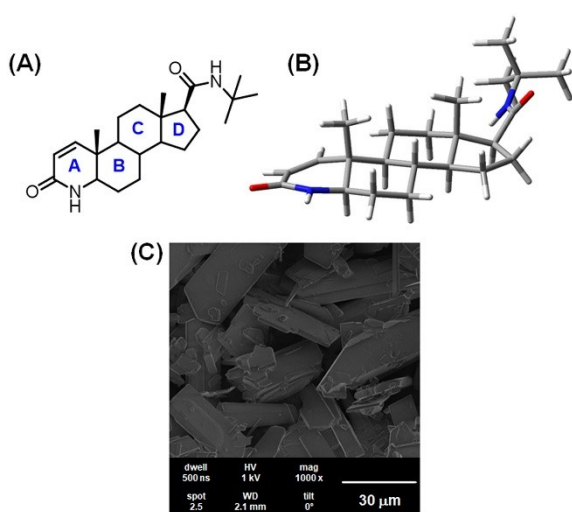


**Figure 1.** A) 2D structure, B) 3D X-ray structure, and C) scanning electron micrographs (SEM) of the crystal form I of finasteride.

## Results and Discussion

The spatial resolution that can be achieved with B23 beamline<sup>[7a]</sup> is currently 50  $\mu\text{m}$ .<sup>[8]</sup> ECD imaging enables the recognition of domains of different supramolecular structure of heterogeneous samples, which would otherwise appear homogeneous using bench-top instruments because of their lower spatial resolution of about 2–3 mm or more.

The synthesis and characterization of the crystal form I of finasteride, *N*-(1,1-dimethylethyl)-3-oxo-4-aza-5 $\alpha$ -androst-1-ene-17 $\beta$ -carboxamide, was reported previously.<sup>[18]</sup> The main chromophore of finasteride is an  $\alpha,\beta$ -unsaturated  $\delta$ -lactam moiety, contained in ring A, which is extremely rigid, similarly as the remaining rings B, C and D. The second chromophore is the amide group located at carbon atom C17 of ring D. For this substituent only a partial rotation around C17–C(=O) bond is expected. This structure allows for only a minimal number of possible conformations so that finasteride creates packing polymorphs.<sup>[18]</sup> As expected, the ECD spectra of the three distinct polymorphs are almost identical making ECD spectroscopy unable to distinguish them.<sup>[18]</sup> This is not the case using vibrational CD (VCD) spectroscopy where different spectral bands observed over the range from 1525 to 1400  $\text{cm}^{-1}$  can be used to discriminate the finasteride polymorphs and used as fingerprints.

The measurements using bench-top ECD instrument revealed that the spectra of pure polymorphic form I of finasteride in KCl pellet (Fin-I-KCl) recorded at 0° and 90° rotation around the propagation direction of the incident light showed a very similar bisignate profile with band A negative and band B positive (Figure 2A). This indicated that linear dichroism (LD) and linear birefringence (LB) contributions to the ECD were negligible. LD spectra of the pellet measured under the same conditions (Figure 2B) showed small differences between 0° and 90° orientation with an overall small intensity magnitude range from  $+2.5 \times 10^{-3}$  to  $-1.0 \times 10^{-3}$   $\Delta\text{OD}$ . For these reasons, the scanned ECD spectrum of Fin-I-KCl can be considered as pure isotropic ECD that, being qualitatively similar to that scanned in acetonitrile (Figure 2A) was indicative of similar molecular conformations in both the solid and

solution states. However, one can see that the solution spectrum recorded in acetonitrile, compared to the solid-state spectrum, shows a blue shift of approximately 10 nm for both bands. A similar phenomenon occurs in the absorption spectrum (Figure S1† in the Supporting Information). This is related mainly to crystal packing effects (solvent-to-crystal shift) and a similar phenomenon has been previously reported in several instances, including compounds with enone-type chromophores measured in acetonitrile and as KCl pellets.<sup>[19]</sup> The similarity between solution and solid-state ECD spectra implies that the intermolecular interactions between closely packed molecules were not affecting the molecular conformation of finasteride, and that the ECD spectrum of Fin-I-KCl is governed by single-molecule effects and not, for example, by intermolecular exciton couplings in the crystal lattice.<sup>[11]</sup>

The ECD spectral features were simulated with quantum mechanical calculations using time-dependent density-functional theory (TDDFT; Figure 2C) and the so-called solid-state ECD/TDDFT approach.<sup>[9b,c,18]</sup> The simulated ECD spectra using the input structure from X-ray crystallographic data, with all H-atoms optimized, were in very good agreement with the observed one with the bench-top instrument. According to TDDFT calculations, bands A and B (Figure 2A) were associated to the electronic transitions 1, 2 and 4 for the  $\alpha,\beta$ -unsaturated lactam moiety and transition 3 for the amide chromophore (Figure 2C).

Following the bench-top ECD measurements, the same Fin-I-KCl pellet was studied by ECD imaging (ECDi) using the highly collimated micro beam of the Diamond B23 beamline. For this measurement, the light beam was focused to a diameter size of  $\sim 0.1$  mm at the sample surface. The investigated sample area of 6 mm  $\times$  6 mm was scanned as a grid of 12 columns by 12 rows at intervals of 0.5 mm corresponding to 144 synchrotron radiation CD (SRCD) spectra scanned in the 200–400 nm wavelength range. The thin pellet was held horizontally on a motorised XY stage (PI Instruments, Germany). The 144 spectra scanned with B23 ECDi showed a very large spectral variability (Figure 3E) unlike those scanned in solution and in the solid-state pellet using the bench-top instrument that were very similar (Figure 2A).

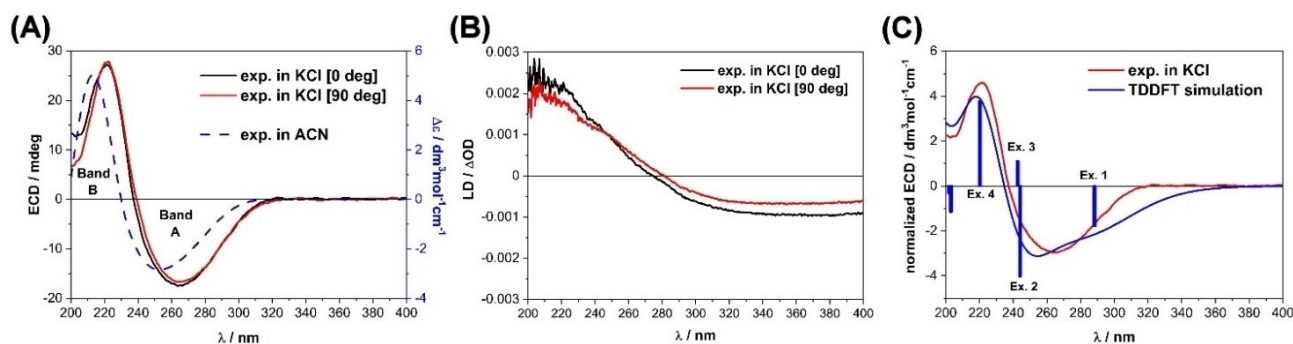


**Figure 2.** A) Solid-state ECD spectra of finasteride in a KCl pellet recorded on a bench-top instrument compared to the solution spectrum recorded in  $\text{CH}_3\text{CN}$ , the blue scale on the right axis corresponds to the  $\text{CH}_3\text{CN}$  spectrum, also shown in blue. B) Solid-state LD and C) solid-state ECD spectrum of finasteride compared with the TDDFT calculations based on X-ray data at the CAM-B3LYP/TZVP level of theory; the simulated curve was generated with  $\sigma = 0.6$  eV. For better comparison with the experiment, the computed curve was divided by 1.5 and red-shifted by 25 nm; vertical bars represent rotational strength values.



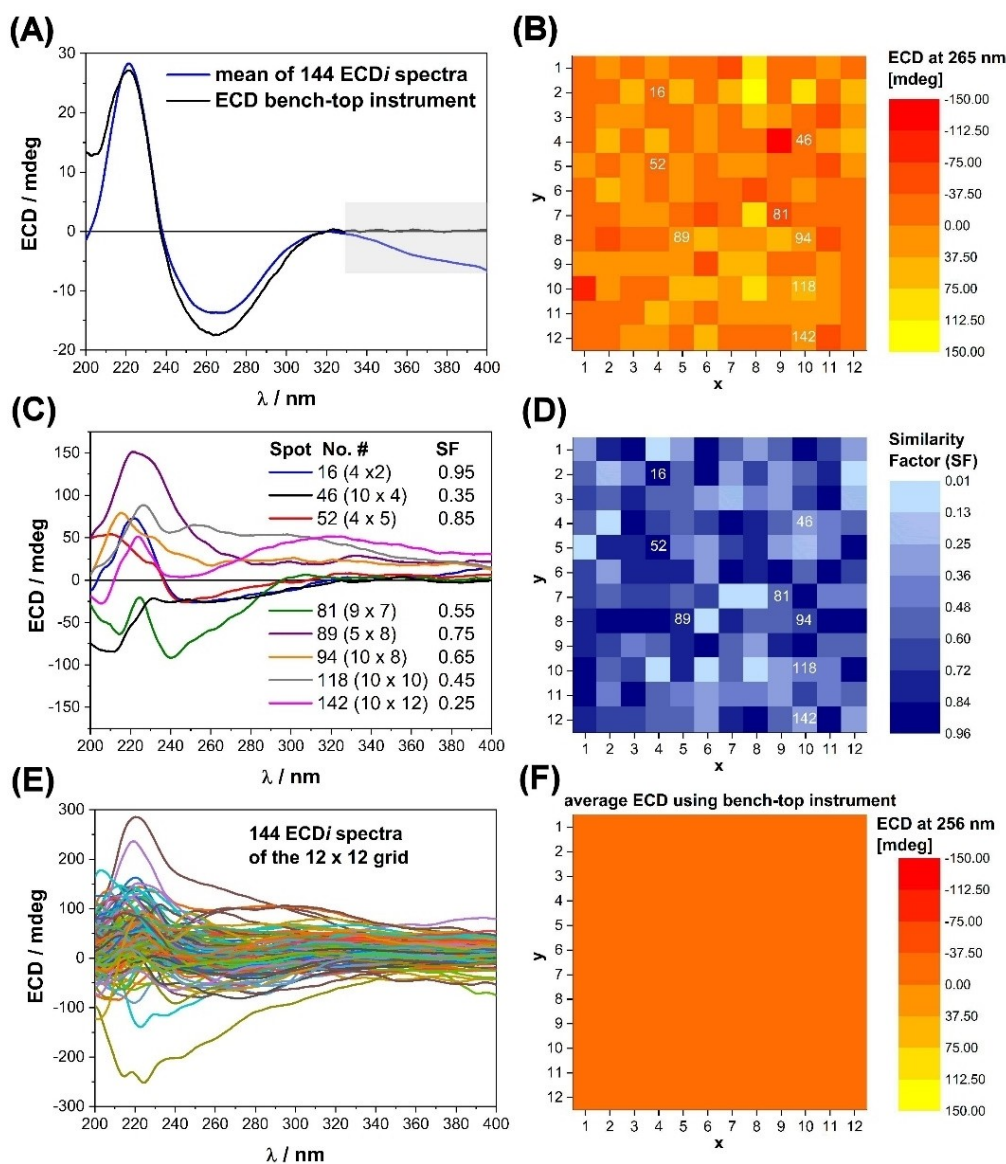


**Figure 3.** A) Comparison of ECD spectrum of Fin-I-KCl recorded with a bench-top instrument with the calculated average spectrum from the 144 ECDi spectra scanned in a  $12 \times 12$  grid area of 0.5 mm step size with a beam diameter of  $\sim 0.1$  mm. Note that the final ECD spectrum is not corrected for scattering effects over the range of 320–400 nm. B) Color map representing the local values of ECDi at 265 nm recorded for the 144 spots of a  $12 \times 12$  grid array with 0.5 mm step size. C) Selected ECDi spectra with their similarity factors (SF). D) Similarity factor map based on the comparison of single ECDi spectra with the ECD spectrum recorded on a bench-top instrument. E) 144 ECD spectra of the  $12 \times 12$  grid at 0.5 mm steps. F) Calculated 2D map at 265 nm from the measured spectrum with bench-top instrument illustrated in Figure 3A. Note: the numbers shown on the individual pixels in (B) and (D) correspond to the numbers of the spectra shown in (C).

It is important to note that the calculated average spectrum (Figure 3A) from the 144 ECDi spectra (Figure 3E) was very similar to those measured with the bench-top instrument both in solution and in the solid state as a pellet (Figure 2A). Also from the CD intensity magnitude at 265 nm of the 144 spectra, the 2D map of the  $12 \times 12$  grid illustrates more clearly the change in sign from positive (yellow hues) to negative (red hues) of the ECD. At visual inspection of the 2D map, 54 points called “pixels” were positive, coloured with yellow hues, 20 were associated with weak signal coloured orange, and 70 were negative coloured in red hues, that were scattered randomly in

the  $6 \times 6$  mm investigated area within the range +150 to –150 mdeg (Figure 3B).

For comparison, the 2D map generated from the ECD intensity of Figure 2A of the spectrum scanned with bench-top instrument would show a uniform orange colour (Figure 3F). For clarity, eight of the 144 ECDi spectra were selected to depict the spectral variability in terms of shape and intensity (Figure 3C).

A very useful method to analyse a large set of ECDi spectra of different spectral shapes and intensity magnitude is provided by the so-called similarity factors (SF) analysis<sup>[20]</sup> where the factor can vary from 0, for no similarity, to 1, for identity. For

the present data, SF quantifies the degree of similarity of each data point of the grid with respect to a reference spectrum for which we chose the isotropic ECD spectrum recorded for the KCl pellet using the bench-top instrument. The distribution of the SFs for the spot measurements in the investigated grid area is shown as a 2D map in Figure 3D where a darker colour indicates higher similarity. This map highlights the huge variations of SF in local ECD spectra and the fact that nearby regions are not correlated with one another, which is consistent with the map of the 2D ECD image in Figure 3B. Similar results were also obtained for a different area of the same pellet (Figure S2†).

The results collected so far demonstrated that the average size of the microcrystallites is below the size of the “pixels”, namely  $0.25 \text{ mm}^2$ , and the microcrystallites are uniformly distributed over the pellet, meaning that there are almost no spots devoid of microcrystallites. The large variation of the ECD spectra, together with the known properties of the solid-state ECD spectrum of finasteride (not affected by conformational factors or intermolecular couplings), is mostly due to ACD, that is, to the different orientation of each crystallite with respect to the incident radiation, which is relevant for the following discussion.

As the focused beam light on the sample surface was about  $100 \mu\text{m}$  diameter, each of the 144 spectra corresponds to the mean of all crystallites from I of finasteride in that spot area. The average of the 144 ECD spectra resembled that of the apparent isotropic CD measured in about 2.7 larger area as illustrated in Figure 3A. To understand what determines this situation, let us start with a very simple model, which will become more sophisticated and closer to reality thereafter. Let us assume that only one electronic transition is the origin of the  $n$  measured ECD spectra of the grid area. Then, the ECD can be expressed as:

$$\Delta\varepsilon = \frac{1}{n} \sum_{j=1}^n \Delta\varepsilon_j^A \quad (3)$$

where  $n$  is the number of spots measured, and  $\Delta\varepsilon^A$  is the (anisotropic) CD associated with each spot.

It appears that with large  $n$ , like in this case with 144 spectra, the average profile is very similar to the isotropic one. However, for small  $n$  (possibly limited to a few units), then  $\Delta\varepsilon$  from Equation (3) could be different than the isotropic average and be dominated by the anisotropic CD components. An important result of this ECD imaging study is that the isotropic ECD measured on the whole pellet is the average of ACD spectra for all possible orientations, meaning that the isotropic CD can be considered to be a true chirality measurement<sup>[10,14b]</sup> to be used for the assignment of the absolute configuration.

In summary, the ECD imaging technique has demonstrated that the CD of the full large  $1 \text{ cm}^2$  area of the samples pellet in the solid state measured with bench-top instruments arises from the average of all the orientations of the fine ground crystals, that with KCl constitute the pellet, which are also consistent with randomly oriented molecules in solution. In turn, this allows a direct comparison with the computational

results obtained from the trace of the rotational strength tensor.<sup>[9c]</sup>

It is important to note that the orientation of the crystallites of a single spot of the grid is random and cannot be controlled or measured. If controlled, it would enable the determination of the orientational coefficients by which each ACD spectrum  $\Delta\varepsilon^A$  could be expressed as a combination of the elements  $\Delta\varepsilon_{\alpha\beta}$  of the second-rank tensor.

To be closer to reality, several electronic transitions have to be considered, each characterized by a rotational strength tensor. Each tensor will be diagonal in its own principal frame, but in the general case there exists no molecular orientation in which all the rotational strength tensors are diagonal. At the same time, the emergent  $\Delta\varepsilon^A$  is the superposition of the contributions from several (possibly all) transitions. The combined effect of these two considerations is that one cannot extract the  $\Delta\varepsilon^A$  tensor elements from the ECD spectra. On the other hand, our experiments on a large number of randomly oriented microcrystallite ensembles lend themselves for a statistical treatment, meaning that each ECD spectrum  $\Delta\varepsilon^A$  can be obtained as a linear combination of the tensor elements.

To extract the required information from the ECD measurements, a singular value decomposition (SVD) analysis was performed (Figure 4). We identified and quantified the main six components responsible for the diversity of the ACD spectra recorded on the grid area of the Fin-I-KCl pellet (Figure 4B). We found that ECD spectra of these single components were very different from one another (Figure 4C). Consistent SVD components were obtained from the analysis of a second ECD map recorded using a different area (Figures S2 and S3†) of the same pellet. The singular values demonstrated that the first six components do indeed contribute extensively to the overall ECD spectrum (Figure 4B). The similarity factor between the observed experimental spectrum and that reconstructed from the first six components is  $\text{SF} = 0.958$ . We can therefore identify these six SVD spectra with a combination of the six expected elements of the ACD tensor. It is important to note that only the symmetric components of the ACD tensors can contribute to the SVD spectra, as the antisymmetric components are averaged to zero (see the Appendix).

In order to further confirm this hypothesis, we pursued a computational analysis based on TDDFT calculations aimed at reproducing the observed spectra. As reported in Figure 2C, a simulated isotropic ECD spectrum of finasteride in the solid state was calculated with the so-called solid-state ECD/TDDFT methodology. By choosing the proper keyword, a full transition analysis was printed [*IOp(9/33) = 1*] by the Gaussian 16 software, which provided the elements of the rotational strength total tensor (dipole velocity gauge), as well as  $\mu\text{m}$  and  $\mu\text{Q}$  components, for each electronic transition. One hundred distinct rotation matrices were randomly generated and applied to the rotational strength tensor by a Fortran routine, and the  $\Delta\varepsilon_{zz}$  element of each rotated tensor was extracted. In the next step, an ECD spectrum was obtained by convoluting a set of Gaussian functions (one for each transition) using a bandwidth  $\sigma = 0.5 \text{ eV}$ . The average of the 100 different ECD spectra is fully consistent with the calculated isotropic ECD spectrum (Fig-

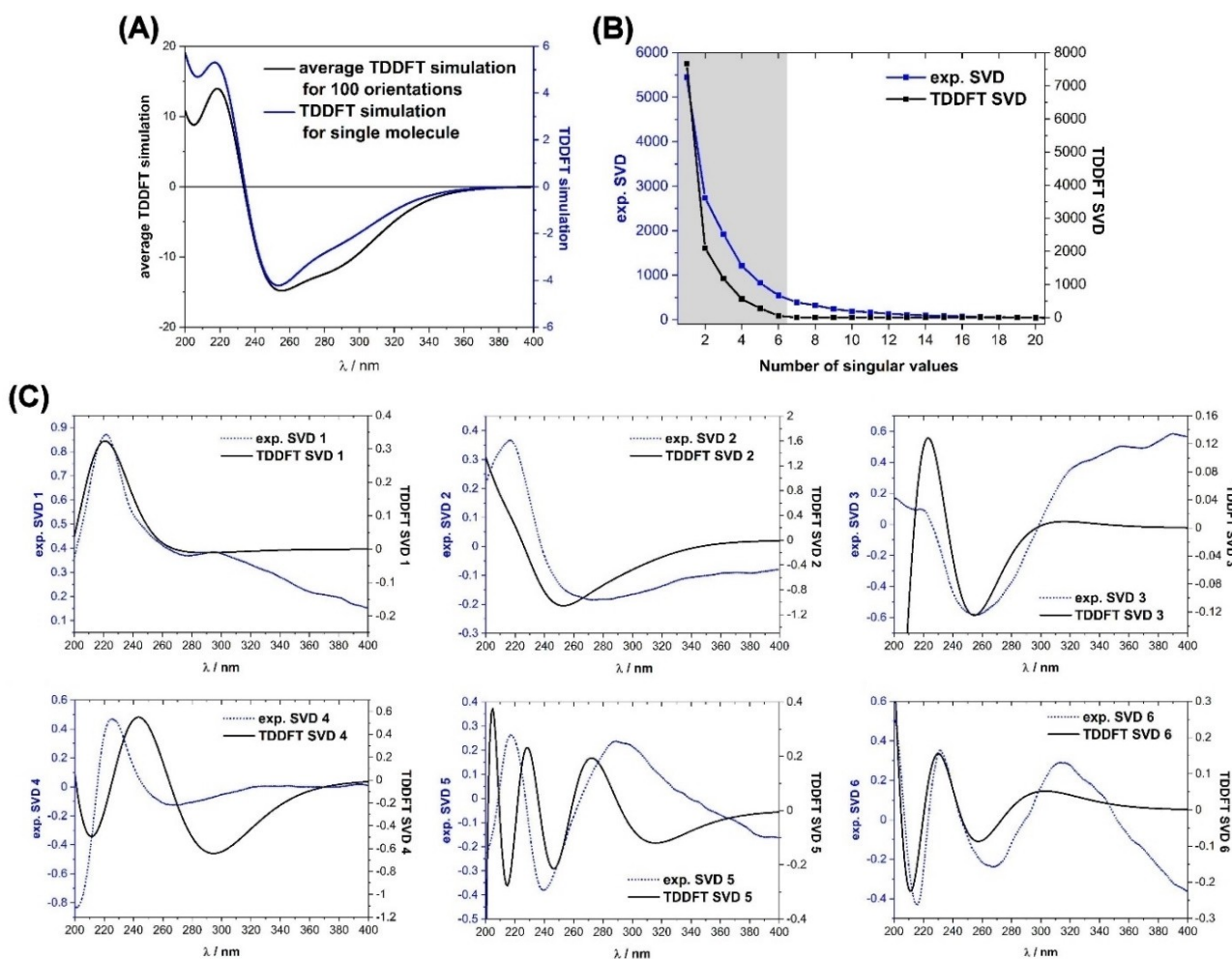


**Figure 4.** A) TDDFT-calculated isotropic ECD spectrum for a single molecule of finasteride compared to the average one calculated for 100 orientations. B) Singular values determined for a map of 144 experimental ECDi spectra and TDDFT calculations of finasteride. C) Comparison of six principal SVD spectral components taken from experimental and calculated data, as described in the text. Note: simulated curves are constructed with  $\sigma = 0.83$  eV and are red-shifted by 25 nm.

ure 4A). Finally, the whole set of spectra was again analysed by SVD. The aim of this procedure was to obtain a set of components to be linked with the experimental ones.

This approach would be equivalent, but much less computationally demanding, to that from a set of TDDFT calculations of randomly oriented structures as visualised in Figure 5, that might in principle be achieved by precluding molecular reorientation using the *nosymm* keyword in the Gaussian 16 software and then extracting the rotational strength tensor components.

The analysis of the singular values indicates that a good reconstruction of the TDDFT ECD spectra was achieved combining only the first six SVD components (Figure 4C). The reconstructed ECD spectrum corresponds with the average one calculated from 100 random orientations of finasteride (Figure 4A, black curve). More importantly, the six SVD components from the TDDFT calculations were in good agreement with the main six SVD components extracted from the ECDi measurements, in particular for SVD2 and SVD4 devoid of light

scattering artifacts (Figure 4C). It is important to notice that this theoretical model does not consider the impact from light scattering or artifacts due to LD.<sup>[21]</sup> The former may be taken as responsible for the significant  $\Delta\epsilon$  intensity values of SVD1, SVD3 and SVD6 in the long wavelength range of 340–400 nm where no electronic transitions occur. Scattering effects are discarded from our consideration, but we do show the long-wavelength range in Figure 4 to give a clear picture of all associated problems. Artifacts arising from the coupling of linear dichroism (LD) with instrumental defects, as well as other anisotropy effects due to a combination of (LD) and linear birefringence (LB),<sup>[12]</sup> could contribute as well to the ECD around 300–320 nm like for SVD5 (Figure 4C). Apart from these discrepancies, the overall agreement between the set of experimental and TDDFT calculated SVD spectra is quite good.

Many stereochemical assignments rely on the comparison between observed and calculated ECD spectra. Our results expand the space for this comparison and to offer a theoretical proof of this, we studied 17-epi finasteride, an epimer of

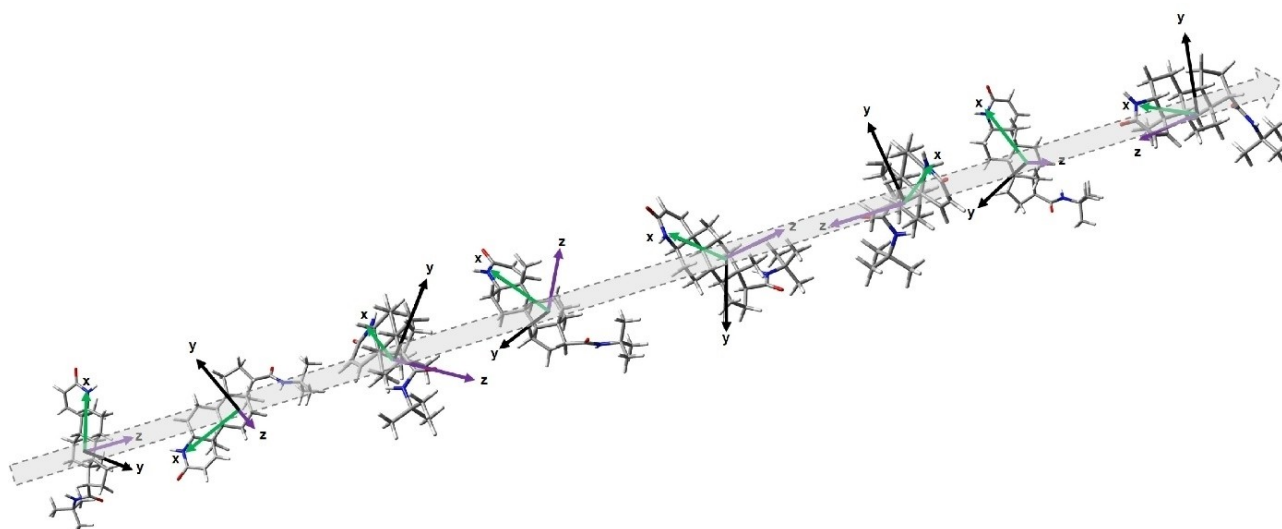


**Figure 5.** Representation of finasteride molecules randomly arranged along the incident light path. The generation of random rotation matrices corresponds to varying the orientation of the principal axes,  $x$ ,  $y$  and  $z$ , of each molecule.

finasteride with inverted configuration at C-17 where the tert-butyl carboxamide is attached. Inversion from  $17\beta$  to  $17\alpha$  configuration completely alters the surrounding of this amide chromophore. Nevertheless, the overall TDDFT-calculated ECD spectrum of 17-epi finasteride was quite similar to that of finasteride (Figure S5†). However, when the computational procedure described above was applied to the isomer, some of the 6 SVD components displayed sizable differences (Figure S6†) from those of finasteride in Figure 4C. In summary, the comparison of a number of ECD spectra rather than a single one is much more informative as a source of structural information.

As Gaussian 16 outputs the components for the two  $\mu\text{m}$  and  $\mu\text{Q}$  tensors, we also reconstructed ECD spectra by applying the SVD procedure to the two sets separately. The results indicate that the  $\mu\text{m}$  contribution overwhelms that of  $\mu\text{Q}$  excluding, at least theoretically, a significant impact from the latter to the ECD of the microcrystalline state that reconciles with that in solution. It is worth noting that the other source of discrepancy, namely intercrystalline exciton-like couplings, may also be quantified through computational means.<sup>[11]</sup>

## Conclusion

The measurement of ECD spectra of microcrystalline compounds mixed with KCl in pellets is a useful method to investigate the stereochemistry of chiral species in the solid state. When determination of an absolute configuration is sought, looking at a crystalline sample rather than one in solution might avoid the need for conformation analyses. Polymorphic forms of chiral compounds, like those of APIs with possible different absorption, distribution, metabolism, excretion (ADME) parameters, may be investigated directly in their pill or tablet form. Some compounds like chiral metal–organic

frameworks (MOFs) and coordination polymers have been found to retain chirality only in the solid state.<sup>[22]</sup>

Samples of microcrystals dispersed in a salt matrix are intrinsically anisotropic. Two approaches can be used. That of Kuball and collaborators measured anisotropic CD (ACD) spectra with a special apparatus and demonstrated the relation with ECD tensor components. The other required ECD spectra of standard pellets measured at various rotations around the axis parallel to the direction of the incident light and also flipped orthogonally to ascertain whether the spectra are unchanged – namely isotropic – or different – namely anisotropic. Here, we have expanded the second approach by demonstrating that local anisotropies of chiral microcrystalline finasteride mixed with KCl average over relatively large areas of the investigated pellets resembling isotropic solution media. This was achieved by ECD imaging using the highly collimated microbeam generated at the Diamond B23 synchrotron beamline.

The ECD spectra were analysed by using the SVD method, and the reconstructed spectra were in good agreement with TDDFT calculations, thus demonstrating that the spectral variation observed when mapping grid areas using the ECD imaging method pioneered at the Diamond B23 beamline were due to the local anisotropies. These local anisotropies were generated by the random orientations of the microcrystallites of the chiral sample mixed with KCl in the pellet, and could only be detected because of the higher spatial resolutions of about  $100\ \mu\text{m}$ , achievable at B23, but unattainable with bench-top instruments. In this manner, the measurement of each grid point of the pellet was revealed to be an ACD spectrum. The averaging of a sufficient number of grid points, each being the average of local microcrystallites orientations within  $100\ \mu\text{m}$ , led to an ECD spectrum that was very similar to that measured in solution. The same average can in turn be related to a calculated isotropic ECD spectrum. The standard pellet technique is fully justified as a source of structural information,



provided that the common procedures for excluding LD-, LB-, and light scattering-related artifacts are followed.

A possible way of reproducing the variability of ACD spectra with computational means is by generating a set of random molecular orientations and fixing them in the calculation. Under these conditions, the program Gaussian 16 we employed for the calculations would provide a different ECD tensor for each orientation. More practically, we generated 100 tensors by applying a random rotation matrix. Although the two sets of spectra, experimental and calculated, cannot be directly compared, application of the SVD procedure led to six component spectra showing a strong resemblance between the calculations and the experiment, apart from scattering effects. From a theoretical viewpoint, these components are a linear combination of the ACD tensors. In general, most of the absolute configuration assignments rely on the comparison between experimental and calculated chiroptical properties from ECD, VCD, and OR data. ECD spectra often suffer from an intrinsically limited small number of bands, unlike with IR/VCD spectroscopy when one talks in fact of a fingerprint region. Our results overcome these limitations for ECD by multiplying the number of spectra suitable for the comparison and providing a kind of ECD fingerprint that can be successfully used to assign the absolute configuration of chiral molecules.

This might be beneficial in a number of controversial situations, for example with compounds that have similar or identical solid-state ECD spectra, also for different isomorphs of a API, or with two epimers of a chiral substance. Such closely related compounds might yield a different set of SVD spectra to be used for their chiroptical characterization as fingerprints. The ECD imaging technique could be also extended to characterise the distribution of APIs in pills or tablets in different pharmaceutical formulations and, by applying the fingerprint concept, to find the producer of the active substance by using a previously constructed database. This might also be profitable for controlling the traffic of illegal substances.

## Experimental Section

### Solid-state ECD measurements

Solid-state sample of form I of finasteride for measurements was prepared using the pellet technique (~0.1 mg powder per 150 mg KCl). The crystalline form I of finasteride was mixed with previously dried KCl, finely grounded in a ball mill (Super-Shak IR SS-01 S.T. Japan Ltd.) for 15 s using 3600 rpm and pressed at 10 tons under vacuum for 3 min to make a 13-mm diameter transparent pellet. Then, the solid-state ECD spectra were recorded between 400–200 nm at room temperature using Jasco J-815 ECD spectropolarimeter. All spectra were obtained using 100 nm/min scanning speed, step size of 0.2 nm, bandwidth of 1 nm, a response time of 0.5 s, an accumulation of 5 scans, a continuous scanning mode and standard sensitivity. The pellet was mounted on a rotatable holder in ECD spectropolarimeter and then several ECD spectra were measured upon rotation of the disk around the incident axis direction at various rotation angles. Moreover, the pellets were measured from the backside. These spectra were almost identical, demonstrating the absence of detectable spectral artifacts.

In the next steps, the same pellet was used for all ECD experiments. ECD mapping was performed under N<sub>2</sub> purging using the end-station B spectrophotometer available at B23 beamline for synchrotron radiation CD (SRCD) of the Diamond Light Source.<sup>[23]</sup> The sample was held horizontally with the vertical incident light passing through the pellet. For each pellet, data were recorded with two different orientations of the pellet, upon flipping it around the vertical axis. The detailed measurement procedure is given in the Results and Discussion section. The raw data were processed and SVD analysis carried out using the B23 software program CDApp.<sup>[24]</sup>

## Computational Details

### Solid-state TDDFT ECD calculations

All calculations were run with the Gaussian 16 suite of programs.<sup>[25]</sup> The calculations were performed using as an input structure the X-ray data for the form I (CSD code<sup>[26]</sup> WOLXOK02) of finasteride. After optimization of hydrogen atoms at B3LYP/6-31G(d) level of theory, ECD/UV spectra were simulated in vacuum using the CAM-B3LYP functional and TZVP basis set. TDDFT calculations were repeated using B3LYP/TZVP level of theory. In all cases, the agreement with experimental data was good. Therefore, we focused only on results obtained from the CAM-B3LYP functional. The geometry of 17-epi-finasteride was generated by that of finasteride by inversion of C-17 chirality centre. The three possible conformers were optimized at the B3LYP/6-31G+(d) level of theory, yielding the conformer shown in Figure S5† as the only populated conformer at 300 K. TDDFT calculations were run at the same CAM-B3LYP/TZVP level of theory.

### SVD analysis

Single value decomposition (SVD) was used as factor analysis of calculated spectra.<sup>[27]</sup> SVD were carried out using an in-house program written in fortran90, that calls the SVD routine DGESVD from the LAPACK libraries. More specifically, the Intel Math Kernel Library (MKL) provided with the Intel Parallel Studio XE 2020 suite of compilers was employed.

### Simulation of anisotropic spectra

The simulation of anisotropic spectra was performed using an in-house fortran90 program. The program reads the total rotational strength tensors (RST) and frequencies of the computed transitions and generates the desired number of random rotation matrices using the following algorithm:

- Three uniformly distributed random numbers are drawn and used as components of a 3x3 skew-symmetric matrix
- The exponential of such a matrix is computed: this is an orthogonal matrix and can be used as a random rotation matrix.

All the RSTs are then rotated and the “zz” component is extracted. The resulting components are used to generate a spectrum as a convolution of Gaussian functions with fixed, given standard deviation.

The code for ACD analysis and example data can be found at <https://github.com/filippolipparini/cdsvd>.

## Appendix

### Proof that there can only be 6 independent components in a simulated anisotropic spectrum

The program described before generates a spectrum, given  $n$  rotation strength tensors and transition frequencies,

$$\sigma(\lambda) = \sum_{k=1}^n [R_k]_{zz} g(\lambda - \lambda_k),$$

Where  $R_k$  is the rotational tensor associated with the  $k$ -th transition and  $g$  is a Gaussian lineshape function. For later convenience, it is worth introducing a tensor function

$$I(\lambda) : \mathbb{R} \rightarrow \mathbb{R}^{3 \times 3}, I(\lambda) = \sum_{k=1}^n R_k g(\lambda - \lambda_k),$$

so that the spectrum  $\sigma(\lambda)$  can be seen as the  $zz$  component of the tensor function  $I$ .

Let us now consider a set of random rotation matrices  $U_i$ ,  $i = 1, N$ . We obtain a spectrum in the random orientation as

$$\sigma_i(\lambda) = \sum_{k=1}^n [U_i^T R_k U_i]_{zz} g(\lambda - \lambda_k) = U_i^T \left[ \sum_{k=1}^n [R_k]_{zz} g(\lambda - \lambda_k) \right] U_i$$

$$= [U_i^T I(\lambda) U_i]_{zz}$$

We want to show that any  $\sigma_i(\lambda)$  can be written as the linear combination of at most 6 independent functions or, in other words, that only the symmetric component of the tensor function  $I$  contributes to the rotated spectrum. Let  $I(\lambda) = S(\lambda) + A(\lambda)$ , where

$$S = \frac{I + I^T}{2}, A = \frac{I - I^T}{2}$$

are the symmetric and antisymmetric components of  $I$ , respectively. We will show that all the diagonal components of  $U_i^T A(\lambda) U_i$  vanish:

$$\begin{aligned} [U_i^T A U_i]_{\alpha\alpha} &= \sum_{\beta\gamma} U_{i,\beta\alpha} A_{\beta\gamma} U_{i,\gamma\alpha} = - \sum_{\beta\gamma} U_{i,\beta\alpha} A_{\gamma\beta} U_{i,\gamma\alpha} \\ &= - \sum_{\beta\gamma} U_{i,\gamma\alpha} A_{\beta\gamma} U_{i,\beta\alpha} = - [U_i^T A U_i]_{\alpha\alpha} \end{aligned}$$

And therefore,  $[U_i^T A U_i]_{\alpha\alpha} = 0$ .

As there are at most six independent components in a symmetric matrix, there are at most six independent functions of which the rotated spectrum can be a linear combination. This explains why when computing the SVD of the computed randomly oriented spectra we find exactly six nonvanishing singular values.

We note that this is of course an idealized situation that assumes that all the spectral lines have exactly the same line shape and that there is no experimental noise of any sort. In a real situation, one can expect to find more nonzero singular values.

## Author Contribution

Conceptualization: M.G., G.P., L.D.B. Formal analysis: M.G., F.L. Investigation: M.G., G.A., F.L., G.P. Methodology: T.J., R.H., G.S. Project administration: G.S., L.D.B. Software: F.L. Supervision: G.S., L.D.B. Visualization: M.G., G.P. Writing – original draft: M.G., G.P., L.D.B. Writing – review & editing: all authors.

## Acknowledgements

Access to the Diamond Light Source B23 beamline was granted under Project SM17621 and SM19225. M.G. thanks the Bekker Program from the Polish National Agency for Academic Exchange (NAWA) and the Polish National Science Centre (NCN) for Sonata grant no. 2019/35/D/ST4/00394. G.P. gratefully acknowledges financial support from the University of Pisa (PRA 2020\_77). The Wrocław Centre for Networking and Supercomputing (WCSS) for computational support is also gratefully acknowledged. The authors acknowledge Prof. Wojciech J. Szczepek for providing a sample of polymorphic form I of finasteride, and Dr. Torsten Bruhn for supplying a development version of the software SpecDis capable of rapid analysis of ECDi maps.

## Conflict of Interest

The authors declare no conflict of interest.

## Data Availability Statement

The data that support the findings of this study are available in the supplementary material of this article.

**Keywords:** active pharmaceutical ingredients · anisotropic circular dichroism · circular dichroism imaging · finasteride · solid-state circular dichroism

- [1] a) N. Berova, L. Di Bari, G. Pescitelli, *Chem. Soc. Rev.* **2007**, *36*, 914–931; b) G. Pescitelli, L. Di Bari, N. Berova, *Chem. Soc. Rev.* **2011**, *40*, 4603–4625.
- [2] H. Yao, E. Wynendaele, X. Xu, A. Kosgei, B. De Spiegeleer, *J. Pharm. Biomed. Anal.* **2018**, *147*, 50–64.
- [3] a) A. Mándi, T. Kurtán, *Nat. Prod. Rep.* **2019**, *36*, 889–918; b) S. Superchi, P. Scafato, M. Górecki, G. Pescitelli, *Curr. Med. Chem.* **2018**, *25*, 287–320; c) L. Grauso, R. Teta, G. Esposito, M. Menna, A. Mangoni, *Nat. Prod. Rep.* **2019**, *36*, 1005–1030.
- [4] a) D. M. Rogers, S. B. Jasim, N. T. Dyer, F. Auvray, M. Réfrégiers, J. D. Hirst, *Chem* **2019**, *5*, 2751–2774; b) J. Kypr, I. Kejnovská, D. Renčíuk, M. Vorlíčková, *Nucleic Acids Res.* **2009**, *37*, 1713–1725.
- [5] a) G. Pescitelli, L. Di Bari, N. Berova, *Chem. Soc. Rev.* **2014**, *43*, 5211–5233; b) G. Albano, G. Pescitelli, L. Di Bari, *Chem. Rev.* **2020**, *120*, 10145–10243.
- [6] M. Srebro-Hooper, J. Autschbach, *Annu. Rev. Phys. Chem.* **2017**, *68*, 399–420.
- [7] a) F. Zinna, C. Resta, M. Górecki, G. Pescitelli, L. Di Bari, T. Jávorfí, R. Hussain, G. Siligardi, *Macromolecules* **2017**, *50*, 2054–2060; b) G. Albano, M. Górecki, G. Pescitelli, L. Di Bari, T. Jávorfí, R. Hussain, G. Siligardi, *New J. Chem.* **2019**, *43*, 14584–14593.

- [8] R. Hussain, T. Jávorfí, G. Siligardi, *Front. Chem.* **2021**, *9*.
- [9] a) J. Frelek, M. Górecki, M. Łaszcz, A. Suszczyńska, E. Vass, W. J. Szczepek, *Chem. Commun.* **2012**, *48*, 5295–5297; b) G. Pescitelli, T. Bruhn, *Chirality* **2016**, *28*, 466–474; c) G. Pescitelli, T. Kurtán, U. Flörke, K. Krohn, *Chirality* **2009**, *21*, E181–E201; d) M. Górecki, *Chirality* **2015**, *27*, 441–448.
- [10] H.-G. Kuball, T. Höfer in *Circular Dichroism of Oriented Molecules* (Eds.: N. Berova, K. Nakanishi, R. W. Woody), Wiley-VCH, New York, **2000**.
- [11] a) D. Padula, S. D. Pietro, M. A. M. Capozzi, C. Cardellicchio, G. Pescitelli, *Chirality* **2014**, *26*, 462–470; b) G. Pescitelli, *Chirality* **2012**, *24*, 718–724; c) G. Pescitelli, *Chirality* **2021**, in press, DOI: 10.1002/chir.23393.
- [12] a) Y. Shindo, M. Nishio, S. Maeda, *Biopolymers* **1990**, *30*, 405–413; b) T. Harada, *Polym. J.* **2018**, *50*, 679–687.
- [13] L. Barron, *Molecular Light Scattering and Optical Activity*, Cambridge University Press, Cambridge, **2004**.
- [14] a) J. Frelek, W. J. Szczepek, S. Neubrech, B. Schultheis, J. Brechtel, H. G. Kuball, *Chem. Eur. J.* **2002**, *8*, 1899–1907; b) H.-G. Kuball, *Enantiomer* **2002**, *7*, 197–205; c) H.-G. Kuball, B. Weiß, A. K. Beck, D. Seebach, *Helv. Chim. Acta* **1997**, *80*, 2507–2514; d) J. Frelek, W. J. Szczepek, H. P. Weiss, G. J. Reiss, W. Frank, J. Brechtel, B. Schultheis, H.-G. Kuball, *J. Am. Chem. Soc.* **1998**, *120*, 7010–7019; e) H. G. Kuball, E. Dorr, T. Höfer, O. Türk, *Monatsh. Chem.* **2005**, *136*, 289–324; f) H.-G. Kuball, B. Schultheis, M. Klasen, J. Frelek, A. Schönhofer, *Tetrahedron: Asymmetry* **1993**, *4*, 517–528; g) H.-G. Kuball, T. Höfer, *Chirality* **2000**, *12*, 278–286.
- [15] A. Matsugaki, H. Takechi, H. Monjushiro, H. Watarai, *Anal. Sci.* **2008**, *24*, 297–300.
- [16] a) Y. Miloslavina, P. H. Lambrev, T. Jávorfí, Z. Várkonyi, V. Karlický, J. S. Wall, G. Hind, G. Garab, *Photosynth. Res.* **2012**, *111*, 29–39; b) J. T. Nielsen, N. V. Kulinskaya, M. Bjerring, J. M. Linnanto, M. Rätsep, M. Ø. Pedersen, P. H. Lambrev, M. Dorogi, G. Garab, K. Thomsen, C. Jegerschöld, N.-U. Frigaard, M. Lindahl, N. C. Nielsen, *Nat. Commun.* **2016**, *7*, 12454; c) P. Akhtar, D. Lindorfer, M. Lingvaj, K. Pawlak, O. Zsiros, G. Siligardi, T. Jávorfí, M. Dorogi, B. Ughy, G. Garab, T. Renger, P. H. Lambrev, *J. Phys. Chem. B* **2019**, *123*, 1090–1098; d) D. Lindorfer, T. Renger, *J. Phys. Chem. B* **2018**, *122*, 2747–2756.
- [17] N. Otberg, A. M. Finner, J. Shapiro, *Endocrinol. Metab. Clin. North Am.* **2007**, *36*, 379–398.
- [18] J. Frelek, M. Górecki, A. Dzedzic, E. Jabłońska, B. Kamieński, R. K. Wojcieszczyk, R. Luboradzki, W. J. Szczepek, *J. Pharm. Sci.* **2015**, *104*, 1650–1657.
- [19] a) N. U. Rehman, H. Hussain, S. Al-Shidhani, S. K. Avula, G. Abbas, M. U. Anwar, M. Górecki, G. Pescitelli, A. Al-Harrasi, *RSC Adv.* **2017**, *7*, 42357–42362; b) T. Kurtán, R. Jia, Y. Li, G. Pescitelli, Y.-W. Guo, *Eur. J. Org. Chem.* **2012**, *2012*, 6722–6728; c) Z. Hassan, H. Hussain, V. U. Ahmad, S. Anjum, G. Pescitelli, T. Kurtán, K. Krohn, *Tetrahedron: Asymmetry* **2007**, *18*, 2905–2909; d) J. Dai, K. Krohn, B. Elsässer, U. Flörke, S. Draeger, B. Schulz, G. Pescitelli, P. Salvadori, S. Antus, T. Kurtán, *Eur. J. Org. Chem.* **2007**, *2007*, 4845–4854.
- [20] T. Bruhn, A. Schaumlöffel, Y. Hemberger, G. Bringmann, *Chirality* **2013**, *25*, 243–249.
- [21] O. Arteaga, B. Kahr, *J. Opt. Soc. Am. B* **2019**, *36*, F72–F83.
- [22] a) D. Shen, J. A. Cooper, P. Li, Q.-H. Guo, K. Cai, X. Wang, H. Wu, H. Chen, L. Zhang, Y. Jiao, Y. Qiu, C. L. Stern, Z. Liu, A. C. H. Sue, Y.-W. Yang, F. M. Alsubaie, O. K. Farha, J. F. Stoddart, *J. Am. Chem. Soc.* **2020**, *142*, 2042–2050; b) X. Han, J. Zhang, J. Huang, X. Wu, D. Yuan, Y. Liu, Y. Cui, *Nat. Commun.* **2018**, *9*, 1294; c) M. Zeng, A. Ren, W. Wu, Y. Zhao, C. Zhan, J. Yao, *Chem. Sci.* **2020**, *11*, 9154–9161.
- [23] R. Hussain, T. Jávorfí, G. Siligardi, *J. Synchrotron Radiat.* **2012**, *19*, 132–135.
- [24] R. Hussain, K. Benning, T. Jávorfí, E. Longo, T. R. Rudd, B. Pulfordand, G. Siligardi, *J. Synchrotron Radiat.* **2015**, *22*, 465–468.
- [25] M. J. Frisch, et al.; *Gaussian 16, Revision C.01*, Gaussian, Inc., Wallingford, CT, **2016**.
- [26] C. R. Groom, I. J. Bruno, M. P. Lightfoot, S. C. Ward, *Acta Crystallogr.* **2016**, *B72*, 171–179.
- [27] H. Yanai, K. Takeuchi, Y. Takane, *Projection Matrices, Generalized Inverse Matrices, and Singular Value Decomposition*, Springer, New York, **2011**.

---

Manuscript received: October 7, 2021

Version of record online: December 21, 2021